A Transition-State Analogue Reduces Protein Dynamics in Hypoxanthine-Guanine Phosphoribosyltransferase †

ARTICLE *in* BIOCHEMISTRY · JULY 2001

Impact Factor: 3.02 · DOI: 10.1021/bi010203f · Source: PubMed

6 AUTHORS, INCLUDING:

Ruth Hogue Angeletti
Albert Einstein College of Medicine
234 PUBLICATIONS **7,363** CITATIONS

A Transition-State Analogue Reduces Protein Dynamics in Hypoxanthine-Guanine Phosphoribosyltransferase†

Fang Wang,‡,§ Wuxian Shi,§ Edward Nieves,‡,§ Ruth H. Angeletti,‡,§,|| Vern L. Schramm,*,§ and Charles Grubmeyer*,⊥

Laboratory for Macromolecular Analysis and Proteomics, Department of Biochemistry, and Department of Developmental and Molecular Biology, Albert Einstein College of Medicine, 1300 Morris Park Avenue, Bronx, New York 10461, and Department of Biochemistry and Fels Research Institute, Temple University School of Medicine, Philadelphia, Pennsylvania 19140

Received January 31, 2001; Revised Manuscript Received April 3, 2001

ABSTRACT: Hypoxanthine-guanine phosphoribosyltransferase (HGPRT) is the key enzyme in purine base salvage in humans and in purine auxotrophs, including *Plasmodium falciparum*, the leading cause of malaria. Hydrogen/deuterium (H/D) exchange into amide bonds, quantitated by on-line HPLC and mass spectrometry, has been used to compare the dynamic and conformational properties of human HGPRT alone, the HGPRT·GMP·Mg^{2+} complex, the HGPRT·IMP·$MgPP_i$ ↔ HGPRT·Hx·MgPRPP equilibrating mixture, and the transition-state analogue complex HGPRT·ImmGP·$MgPP_i$. The rate and extent of H/D exchange of 26 peptic peptides, spanning 91% of the primary structure, have been monitored. Human HGPRT has 207 amide H/D exchange sites. After 1 h in D_2O, HGPRT alone exchanges 160, HGPRT·GMP·Mg^{2+} exchanges 154, the equilibrium complex exchanges 139, and the transition-state analogue complex exchanges 126 of these amide protons. H/D exchange rates are correlated with structure for peptides in (1) catalytic site loops, (2) a connected peptide of the subunit interface of the tetramer, and (3) a loop buried in the catalytic site. Structural properties related to H/D exchange are defined from crystallographic studies of the HGPRT·GMP·Mg^{2+} and HGPRT·ImmGP·$MgPP_i$ complexes. Transition-state analogue binding strengthens the interaction between subunits and tightens the catalytic site loops. The solvent exchange dynamics in specific peptides correlates with hydrogen bond patterns, solvent access, crystallographic *B*-factors, and ligand exchange rates. Solvent exchange reveals loop dynamics in the free enzyme, Michaelis complexes, and the complex with the bound transition-state analogue. Proton transfer paths, rather than dynamic motion, are required to explain exchange into a buried catalytic site peptide in the complex with the bound transition-state analogue.

Enzymes achieve catalysis by sequential steps leading to and from a catalytically favorable transition state (*1*). Dynamic interactions between the enzyme and substrate vary through the reaction coordinate, and are proposed to be most restrictive in the transition-state complex, leading to rate enhancements of up to 10^{20} relative to the rates of uncatalyzed reactions (*2*, *3*).

A specific question for complexes leading to the transition state is the freedom of motion and access to solvent for peptides engaging in substrate and transition-state interactions. We are interested in measuring the extent to which enzymatic peptides exhibit altered mobility through the reaction coordinate. Many enzymes contain catalytically important peptide loops that are highly mobile, and their immobilization has been proposed in complexes related to the transition state. Crystallographic *B*-factors provide a time-averaged estimate of mobility, but do not distinguish two-state conformations where one occurs with a relatively low probability (e.g., 10%). Crystal lattice contacts can also constrain movement within the protein (*4*). Rates of solvent hydrogen/deuterium (H/D) exchange afford a dynamic, solution-based, measure of loop immobilization, since solvent exchange into peptide bonds includes all conformational access to solvent (*5*). Comparison of solvent exchange rates in complexes that have also been characterized by X-ray crystallography permits dissection of structural factors contributing to exchange rates.

Mass spectrometry (MS)[1] coupled with H/D exchange has been used to study protein conformational changes for nearly a decade (*5*, *6*). The practical methods have been reviewed by Engen and Smith (*7*). Deuterium exchange coupled with MS has been used to investigate folding, unfolding, conformational changes, structural heterogeneity, and the effects of binding or aggregation (*8*). An excellent example is the H/D exchange results of human recombinant (C22A) FK506-

† This work was supported by research grants from the National Institutes of Health (C.G. and V.L.S.). The mass spectrometry facility at AECOM is supported by Facility Grants RR09113 from the NIH and BIR9318193 from the National Science Foundation (R.H.A.).

* To whom correspondence should be addressed. C.G.: Department of Biochemistry, Temple University School of Medicine, 3400 N. Broad St., Philadelphia, PA 19140; e-mail, ctg@ariel.fels.temple.edu; phone, (215) 707-4495. V.L.S.: Department of Biochemistry, Albert Einstein College of Medicine, 1300 Morris Park Ave., Bronx, NY 10461; e-mail, vern@aecom.yu.edu; phone, (718) 430-2813.

‡ Laboratory for Macromolecular Analysis and Proteomics, Albert Einstein College of Medicine.

§ Department of Biochemistry, Albert Einstein College of Medicine.

|| Department of Developmental and Molecular Biology, Albert Einstein College of Medicine.

⊥ Temple University School of Medicine.

10.1021/bi010203f CCC: $20.00
Published on Web 06/13/2001

binding protein detected by MS. These results have been compared in detail with NMR studies (*9*).

N-Ribosyltransferases stabilize transition states with oxocarbenium ion character, varying from fully dissociative for nucleic acid-processing enzymes to more moderately dissociative in the case of purine nucleoside phosphorylase and phosphoribosyltransferases (e.g., refs *10* and *11*). The C-nucleosidic iminoribitol transition-state analogues, the Immucillins, are potent (picomolar to nanomolar) transition-state analogue inhibitors for the *N*-ribosyltransferases. The Immucillins crystallize readily with their target enzymes in complexes that mimic the transition state (*4*, *12*, *13*). Complexes of purine nucleoside phosphorylase (PNP) with Immucillin-H have recently been studied using H/D exchange to demonstrate that the solvent accessibility of PNP is remarkably reduced in the PNP·Immucillin-H·PO_4 complex (*14*). Here, we extend these studies to a key enzyme of purine salvage and recycling.

Hypoxanthine-guanine phosphoribosyltransferase (HGPRT) is a key enzyme in the salvage pathway for purine nucleotide formation in humans, and is the major or sole route for purine nucleotide uptake in some parasitic protozoa, including *Plasmodium falciparum*, the most virulent infective agent of malaria (*15*−*17*). HGPRT catalyzes the reversible Mg^{2+}-dependent transfer of the 5-phosphoribosyl group from α-D-phosphoribosyl-1-pyrophosphate (PRPP) to N9 of the base hypoxanthine or guanine to form nucleotide IMP or GMP, respectively (Figure 1A; *18*). The Immucillin phosphates ImmGP and ImmHP provide powerful and specific inhibition of both human and malarial HGPRTases (*19*), and are candidates for species-specific antibiotics against parasitic protozoa. ^{1}H NMR spectra of the complex of HGPRT with the transition-state analogues reveal strongly deshielded protons that are shifted from resonances seen with the Michaelis complex or with the enzyme alone (*19*). The crystal structures of *Plasmodium* and human HGPRTases with bound transition-state analogues show that a disordered catalytic loop moves ∼25 Å to cover the active site and becomes an ordered two-stranded, antiparallel β-sheet (*12*), as compared to its disordered state in the human HGPRT·GMP·Mg^{2+} complex (Figure 1B,C; *12*, *13*, *20*). In the enzyme with empty or partially filled sites, this loop cannot be identified in the electron density, or is in an intermediate position, surrounded by solvent. A highly conserved serine-tyrosine dipeptide in this loop interacts with the bound $MgPP_i$ and 5′-phosphate groups of the human HGPRT·ImmGP·$MgPP_i$ complex and is known to provide at least 6.5 kcal/mol of stabilization of the transition state for phosphoribosyl group transfer (*21*). Although the catalytic loop (also termed the "flexible loop" or "loop 3") provides the most apparent motion in HGPRT, several other loops have been shown to make significant movements between various liganded states of HGPRT and the complex with transition-state analogues (*22*, *23*).

[1] Abbreviations: DTT, dithiothreitol; fwhm, full width at half-maximum; GMP, guanosine 5′-monophosphate; HGPRT, hypoxanthine-guanine phosphoribosyltransferase; HPP, 7-hydroxy[4,3-*d*]pyrazolopyrimidine; Hx, hypoxanthine; ImmGP, ImmucillinGP; IMP, inosine 5′-monophosphate; LC−MS, high-performance liquid chromatography coupled with mass spectrometry; MS, mass spectrometry; MS/MS, tandem mass spectrometry; PNP, purine nucleoside phosphorylase; PP_i, inorganic pyrophosphate; PRPP, α-D-5-phosphoribosyl-1-pyrophosphate; peptic peptide, HGPRT peptides from pepsinhydrolysis.

Here, we have used H/D exchange to document the changes in global solvent accessibility in four forms of human HGPRTase. Three enzymatic conformational states are explored by analysis of specific peptides. The first is a partially filled catalytic site containing Mg^{2+} and GMP. The second involves an internally equilibrating Michaelis complex of the same enzyme, in which bound IMP and $MgPP_i$ are being interconverted to bound hypoxanthine and Mg-PRPP. The known kinetic parameters permit sequestration of >99% of the enzyme in these forms (*18*). Finally, HGPRT is converted to a conformation proposed to resemble the transition state in the HGPRT·ImmGP·$MgPP_i$ complex (*13*, *19*). Crystallographic studies reveal that this form of the enzyme enjoys the most compact loop interactions with the catalytic site, and the shortest hydrogen bonds between protein groups and catalytic site ligands (Figure 1B; *13*). The catalytic loop, other regions within the active site, and peptides at the subunit interface all undergo reduction in the level of H/D exchange, indicative of sequestration from solvent.

MATERIALS AND METHODS

Human HGPRT and Its Complexes. Construction of the cDNA clone of the human hypoxanthine-guanine phosphoribosyltransferase (HGPRT) from pHPT31 has been reported previously (*20*, *24*). Recombinant human HGPRT was expressed and purified to homogeneity as described previously (*18*, *19*). The purification method yields an enzyme with undetectable alkaline phosphatase activity, permitting incubations with nucleotide ligands without phosphate loss.

Purified HGPRT (11 mg/mL) was stored at 4 °C in 0.1 M Tris-HCl (pH 7.4) containing ammonium sulfate at 70% saturation. Enzyme solutions were desalted prior to experiments by centrifuging the suspension and dissolving the precipitate in 0.1 M Tris-HCl (pH 7.4) containing 5 mM DTT. The ammonium sulfate was removed with a Sephadex G-50 spin column equilibrated in the same buffer (*25*). The HGPRT concentration was 440 μM subunit (10.75 mg/mL) following desalting. The HGPRT·ImmGP·$MgPP_i$ complex and the equilibrium mixture of the Michaelis complexes were formed by incubating 360 μM HGPRT with 2 mM $MgCl_2$, 1 mM PP_i, and either 0.66 mM ImmGP or 1 mM IMP in 0.1 M Tris-HCl (pH 7.4) containing 5 mM DTT for at least 1 h at 4 °C. The HGPRT·GMP·Mg^{2+} complex was formed by incubating 360 μM HGPRT with 1 mM GMP and 2 mM $MgCl_2$ in 0.1 M Tris-HCl (pH 7.4) containing 5 mM DTT for 1 h at 4 °C.

Materials. Pepsin was obtained from Worthington Biochemical Co. (Freehold, NJ), and D_2O (99.9 at. % D) was from Isotec Inc. (Miamisburg, OH). ImmGP was synthesized by published methods (*26*, *27*), and was provided by P. C. Tyler and R. H. Furneaux of Industrial Research Ltd. (Lower Hutt, New Zealand). All other chemicals and reagents were of the highest grade commercially available.

Exchange Studies. H/D exchange from solvent was initiated by dilution of 5 μL of 360 μM HGPRT or its complexes into 95 μL of the corresponding deuterated buffer in >99 at. % D_2O (pD 7.4) to give a final HGPRT concentration of 18 μM. The deuterated buffer for H/D exchange for the HGPRT·ImmGP·$MgPP_i$ complex and the equilibrium mixture for the Michaelis complex also contained 2 mM $MgCl_2$

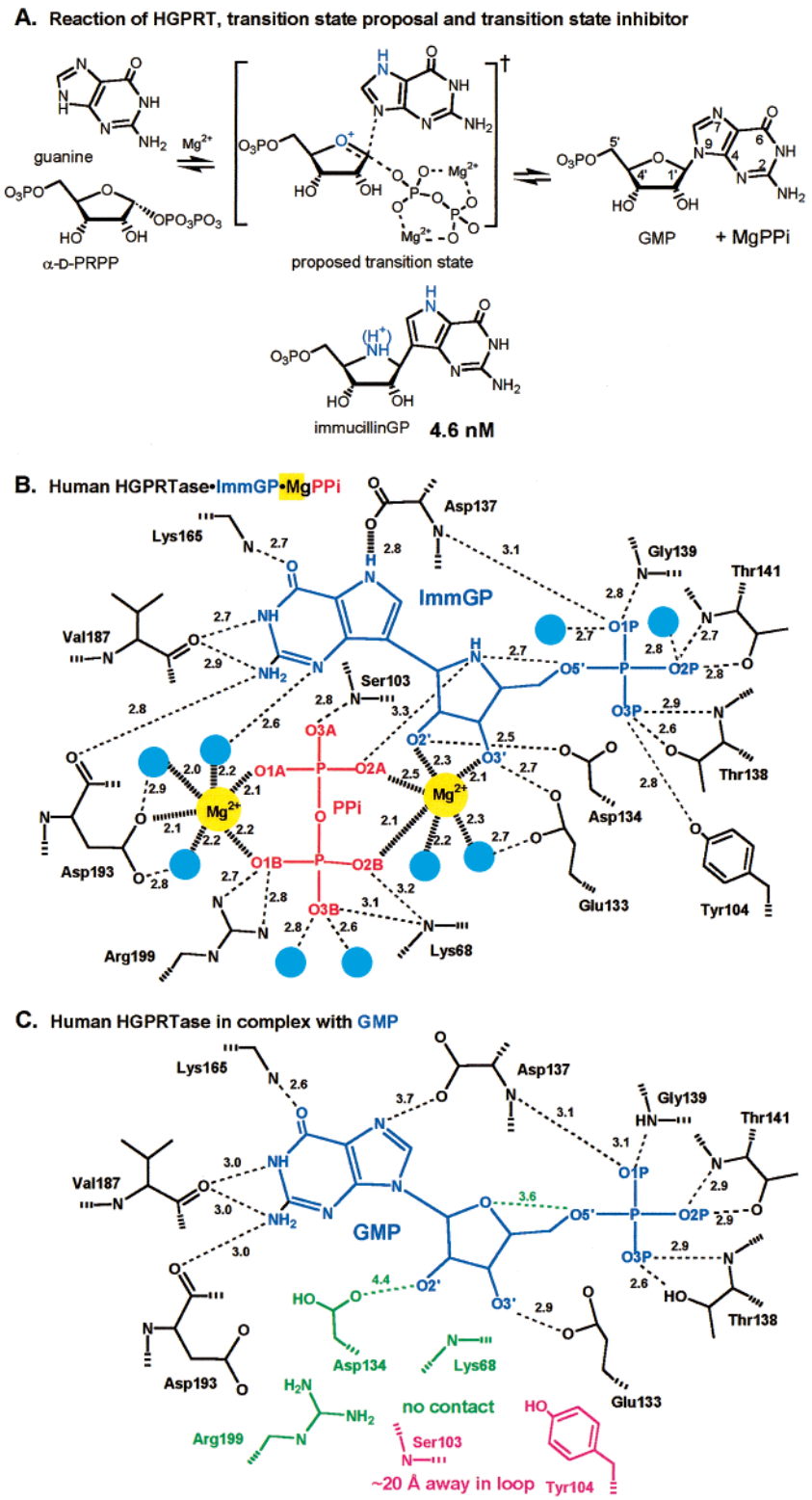

FIGURE 1: (A) Reaction catalyzed by HGPRT. The oxocarbenium ion character of the transition state is proposed from the kinetic isotope effect studies on orotate phosphoribosyltransferase (*38*). The structural features of the transition-state inhibitor, Immucillin-GP, that mimic those of the proposed transition state are shown in blue. (B) Cartoon of active site interactions in the HGPRT·ImmGP·$MgPP_i$ complex (*13*; PDB entry 1BZY). Bound ImmGP is purple. PP_i is red. Mg^{2+} ions are yellow. Water molecules are blue. Two water molecules mentioned in the text are in contact with O1P and O2P. (C) Cartoon of active site interactions in the HGPRT·GMP·Mg^{2+} complex (*20*; PDB entry 1HMP). Bound GMP is purple. Residues Asp134, Arg199, and Lys68, which form contacts in the ImmGP complex, but not the GMP complex, are green. Residues Ser103 and Tyr104 from the loop (25 Å distant in this complex) are magenta. Waters and the catalytic site location of Mg^{2+} were not resolved in this structure.

and 1 mM pyrophosphate. The equilibrium mixture of Michaelis complexes also contained 1 mM IMP for maintaining substrate saturation of the enzyme complex. For H/D exchange of the HGPRT·GMP·Mg^{2+} complex, 1 mM GMP and 2 mM $MgCl_2$ were present in the deuterated buffer. H/D exchange solutions were maintained at 25 °C using a water

bath, and allowed to exchange for different periods of time. At appropriate time intervals, 20 μL of the HGPRT solution was removed from the labeling solution, adjusted to pH 2.4 by the addition of an equal volume of 0.5 M cold ammonium phosphate (0 °C, pH 2.4, 1:1 H_2O:D_2O ratio), and immediately subjected to LC−MS analysis or peptic digestion and subsequent LC−MS analysis to determine the extent of deuterium incorporation into HGPRT or its peptic peptides. For analysis of peptides, exchanged solutions of HGPRT were simultaneously quenched and digested by adding an equal volume of 0.5 M ammonium phosphate buffer (pH 2.4) containing 22 μM pepsin, followed by incubation for 5 min at 0 °C to effect proteolysis prior to LC−MS analysis. Maximally exchanged enzyme samples were obtained by incubation of HGPRT in buffered D_2O without catalytic site ligands for 4 h at 60 °C. The enzyme is known, from kinetic analysis, to be stable to these incubation conditions (*18*).

LC−MS Analysis of Deuterated HGPRT. The extent of deuterium incorporation into HGPRT or its peptic peptides was determined by LC−MS analysis of deuterated HGPRT. An HP 1100 HPLC system equipped with a degasser and a binary pump was employed. The solvent cooling loop (33 in. long with an inner diameter of 0.005 in.), injector, and column were immersed in an ice bath (0 °C) to minimize D/H exchange with HPLC solvents during chromatography. The exchanged and quenched protein solution (5 μL) or peptic digests (20 μL) were loaded onto a Vydac (Separations Group, Hesperia, CA) 1.0 mm × 50 mm C_4 or 1.0 mm × 50 mm C_8 column. Solvent A was 5% acetonitrile in water containing 0.05% trifluoroacetic acid, and solvent B was 95% acetonitrile containing 4.95% H_2O and 0.05% trifluoroacetic acid. Intact HGPRT was eluted with a 2 min gradient from 5 to 90% B. The peptic peptides of HGPRT were eluted with a 0.3 min gradient from 5 to 15% B, followed by an 8 min gradient from 15 to 55% B. In each case, additional solvent volume between the gradient mixer and the column gave rise to an approximate 8.5 min residence time for the protein and peptides on the column. The column effluent (50 μL/min) was delivered directly to a quadrupole ion trap mass spectrometer without flow splitting.

The extent of deuterium exchange was calculated from the mass of the peptide or protein, and the maximal or total exchangeable deuteriums (*5*). Perdeuterated HGPRT (maximally exchanged HGPRT) was obtained by incubating HGPRT in deuterated buffer (pD 7.4) at 60 °C for 4 h. The extent of deuterium loss (back exchange) experienced by the protein or peptic peptides during sample preparation was quantitated from the theoretical mass for the completely amide-deuterated samples compared to the experimental mass determined after LC−MS analysis. The extent of deuterium loss for the intact enzyme was ca. 30% and for its peptic peptides was ca. 40−60%, consistent with previous reports (*28*−*31*). As an example, Figure 2 shows the mass spectral peaks of the HGPRT peptide, L78−F98 $[M + 2H]^{2+}$ ions, following various periods of solution-phase H/D exchange. One stack of peaks is for masses as deuterium exchanges into the HGPRT·GMP·Mg^{2+} complex, and the other is for exchange into the HGPRT·ImmGP·$MgPP_i$ complex. Measurement error in the mass of peptides, and thus determination of the number of deuteriums that are incorporated, is ±0.4 amu ($n = 9$), consistent with the previous reports (*6*, *29*, *30*). The legend of Figure 2 provides information

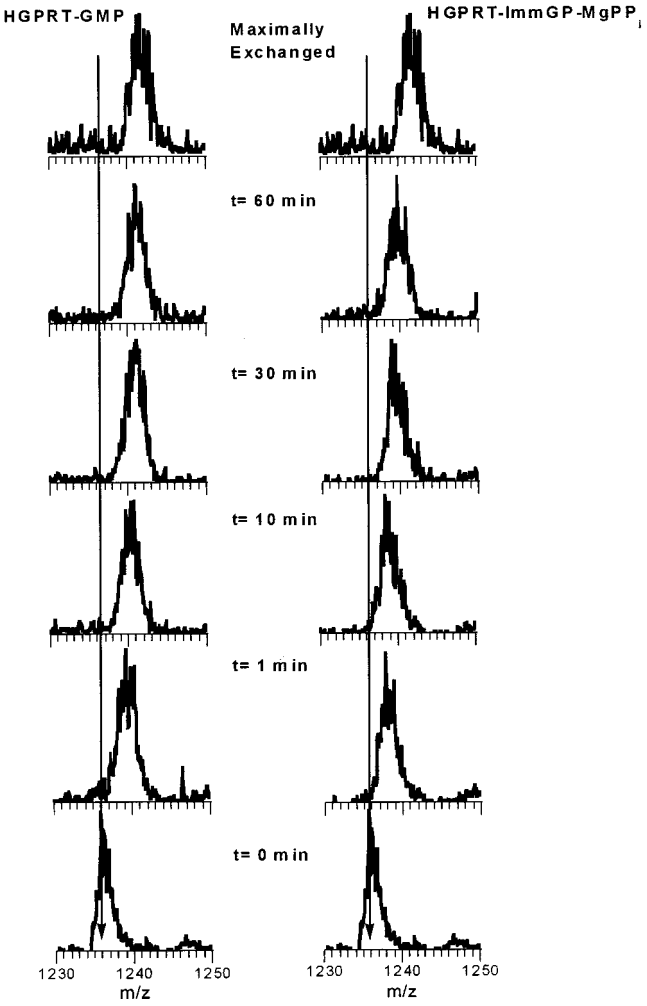

FIGURE 2: Molecular mass analysis (*m*/*z*) for peptide L78−F98 of HGPRT as a function of time in buffered D_2O. The bottom panel ($t = 0$ min) is control peptide (HGPRT added directly to D_2O containing the quench solution at pH 2.4 and 0 °C) with the same sample serving as a starting point for both exchange conditions. Exchange of D_2O was accomplished in buffered solutions of GMP and $MgCl_2$ (left plots, labeled HGPRT-GMP) or in the presence of ImmGP, $MgCl_2$, and inorganic pyrophosphate (right plots, labeled HGPRT-ImmGP-$MgPP_i$) as described in Materials and Methods. The top panel (Maximally Exchanged) is the control sample obtained after incubation for 4 h at 60 °C in buffered D_2O. Note that the top and bottom control panels are duplicates from the same samples. The vertical arrows represent the peptide mass of 1236 at time zero, and the shift to higher mass is deuterium exchange into the peptide backbone.

pertinent to the peptide-specific kinetics of deuterium exchange.

Identification of Peptic Peptides. Peptides of HGPRT were generated with pepsin (1:1.2 substrate:protease molar ratio) at pH 2.4 and 0 °C, by incubation for 5 min in the sample loop of the injector. Peptic peptides were identified either by on-line LC−MS/MS, by off-line HPLC fraction collection followed by MS/MS, or by accurate monoisotopic mass measurement by LC−MS. First, the mass-to-charge ratio (*m*/*z*) of each peptide ion is recorded with no H/D exchange. Tandem mass spectrometry and accurate mass measurements were used to identify each peptide. This procedure is unequivocal for the sequence of the HGPRT protein. Then, the *m*/*z* values of the 26 peptides derived from HGPRT are recorded at exchange times of 0, 1, 3, 10, 30, and 60 min, and for the maximally exchanged conditions. The extent of

deuterium incorporation is then plotted as a function of time for each peptide.

On-line LC−MS/MS was performed on a quadrupole ion trap mass spectrometer, which was operated in a "data-dependent" fashion. The mass spectrometer detected the total intensity of the ions in the *m*/*z* range of 400−2000, and was switched to the mass scanning mode once the ion intensity exceeded a preset threshold. Mass scanning was followed by collision-induced dissociation to acquire a MS/MS spectrum on the most intense ion within a peak during the LC run. The mass isolation window was set at 2 mass units, and the relative collision energy scale was set arbitrarily at 60%. MS/MS spectra were interpreted with searches of peptide databases using the SEQUEST algorithm (*32*). Accurate monoisotopic mass measurement was performed on a quadrupole time-of-flight mass spectrometer with internal calibration by known peptic peptides that were identified by MS/MS. The quadrupole time-of-flight mass spectrometer was tuned to provide a mass resolving power of ca. 5600 fwhm using angiotensin I as the mass standard.

Mass Spectrometry. Mass analyses of deuterated protein and its peptic peptides were performed on a ThermoQuest (Riviera Beach, FL) LCQ quadrupole ion trap mass spectrometer coupled on-line with an HPLC system. The discrete mass spectrum was processed into a peak list, which was further analyzed with MagTran 1.0 software to determine the centroid value for each peak. Accurate mass measurements of peptic peptides were performed on an Applied Biosystems (Foster City, CA) Mariner quadrupole time-of-flight mass spectrometer.

RESULTS

Global H/D Exchange with Intact Human HGPRT. The single polypeptide chain of human HGPRT contains 217 amino acids (*33*) with a molecular mass of 24 448.2 Da. The protein has 207 exchangeable amide protons after correction for the nine proline residues (which lack exchangeable amide hydrogen atoms). Homogeneous HGPRT is stable and remains tetrameric in solution under the H/D exchange conditions described here (*34*).

Global exchange of deuterium into intact HGPRT was performed on four forms of the enzyme. The first and most open form has no catalytic site ligands. The HGPRT·GMP·Mg^{2+} complex has been characterized by crystallography and provides a partially occupied catalytic site (Figure 1C; *20*). A fully occupied and actively equilibrating Michaelis complex (E·IMP·$MgPP_i$ ↔ E·Hx·MgPRPP) was generated by mixing HGPRT with IMP, $MgCl_2$, and pyrophosphate (PP_i). Similar complexes were previously shown to remain active on prolonged incubation (*18*). Under the conditions of equilibration, 94% of the enzyme is in the E·IMP·$MgPP_i$ form, 6% is in the HGPRT·Hx·MgPRPP form, and less than 1% is free (*18*). The final enzyme form, the transition-state analogue HGPRT·ImmGP·$MgPP_i$ complex, forms only in the presence of both Mg^{2+} and PP_i and has been well characterized by X-ray diffraction and NMR (*13*, *19*).

The rate and extent of deuterium incorporation into intact HGPRT were similar for the unliganded enzyme and for the HGPRT·GMP·Mg^{2+} complex. A total of 160 amide hydrogens were replaced in 60 min with deuterium atoms in the free enzyme and 154 in the HGPRT·GMP·Mg^{2+} complex

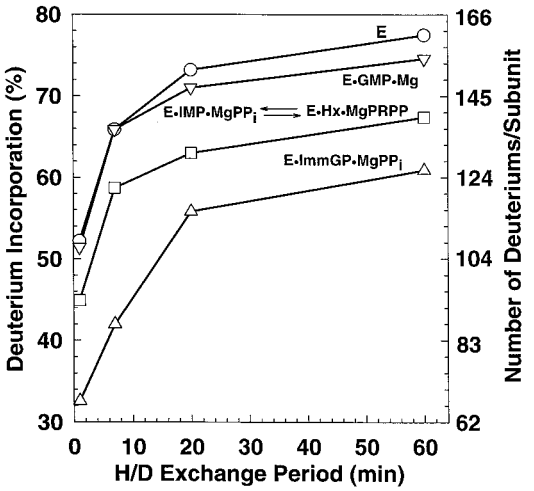

FIGURE 3: Deuterium incorporation into intact HGPRT as a function of time in D_2O. Exchange was accomplished for HGPRT without ligands (○) and HGPRT in the presence of GMP and Mg^{2+} (▽), IMP and $MgPP_i$ (□), or ImmucillinGP and $MgPP_i$ (△).

(Figure 3). Thus, 45 amide hydrogens were unexchanged in HGPRT and 53 in the HGPRT·GMP·Mg^{2+} complex. The extent of deuterium incorporation into HGPRT decreased in the equilibrium mixture of the Michaelis complexes and in the transition-state analogue complex. After the 60 min solvent exchange period, 139 amide hydrogens were exchanged in the equilibrium mixture of the Michaelis complexes and 126 in the HGPRT·ImmGP·$MgPP_i$ complex. Therefore, binding of ImmGP to HGPRT protected 34 exchangeable amide hydrogens of each subunit against solvent exchange compared to free enzyme, and protected 13 sites relative to the equilibrating Michaelis complex. The exchange kinetics indicate that this protection from solvent exchange is primarily the result of the specific prevention of individual amide/solvent exchanges, rather than a globally slower exchange rate.

H/D Exchange of Peptic Peptides of HGPRT. Ligand-induced differences in the solvent accessibility of HGPRT were localized within specific regions of the protein by stopping H/D exchange with acid, followed by rapid pepsin digestion of HGPRT. The local exchange protocol identified 26 peptic peptides by tandem mass spectrometry (MS/MS) (*14*, *30*) or by accurate monoisotopic mass measurement (*31*). These peptides covered 91.2% of the primary structure of the enzyme (Figure 4). H/D exchange into peptic peptides of HGPRT was performed on the HGPRT·GMP·Mg^{2+} complex, the equilibrium mixture of Michaelis complexes, and the transition-state analogue inhibitor complex of the enzyme, for which X-ray structures are available. No significant differences in the extent of deuterium incorporation for these ligation states were observed for 15 peptides (solid lines in Figure 4). Differences in the rate and extent of deuterium exchange into 11 peptic peptides occurred in the transition-state analogue complex and/or in the equilibrium mixture of Michaelis complexes of HGPRT and in the GMP-bound form (dotted lines in Figure 4). The rate constants and extent of H/D exchange into peptides (residues 78−98, 99−121, and 131−145) were dependent on catalytic site ligands (Figure 5). The exchange rates for the peptides show distinct rate patterns in time-dependent maximum entropy analysis (*9*; Figure 6). The number of exchangeable

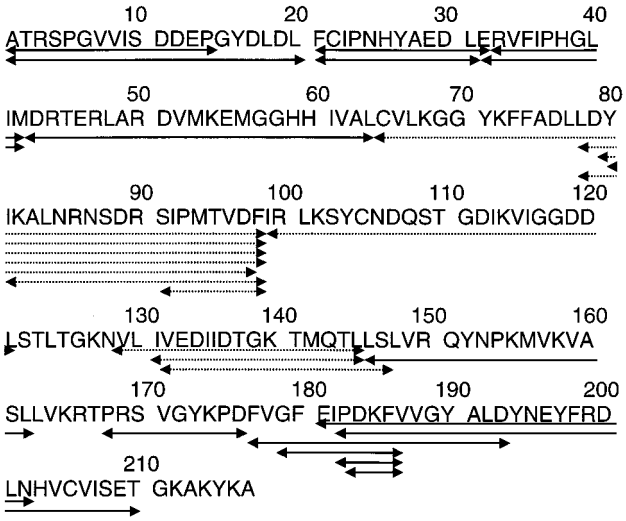

FIGURE 4: Amino acid sequence of HGPRT, indicating the positions of identified peptides for which the extent of deuterium incorporation was measured. Solid lines represent peptides whose exchange rate and extent undergo no change in the transition-state analogue complex compared to those in the HGPRT·GMP·Mg^{2+} complex. Dotted lines represent peptides whose exchange rate and extent change significantly in the transition-state analogue complex compared to those in the HGPRT·GMP·Mg^{2+} complex.

amide hydrogens for each distinguishable rate constant range is indicated in Table 1.

Exchange in Peptide L78−F98. The extent of deuterium incorporation into this peptide decreases in the equilibrating Michaelis complex as well as in the transition-state analogue complex, compared to the level in the HGPRT·GMP·Mg^{2+} complex (Figure 5A). After a 60 min period of exchange, three additional amide protons of peptide L78−F98 are protected in the equilibrating Michaelis complex and five in the transition-state analogue complex. Binding the transition-state analogue protects two additional protons from solvent access relative to the equilibrating complex. One amide hydrogen with a very fast exchange rate ($k > 100$ h^{-1}) and another with a medium exchange rate (1 $h^{-1} < k < 10$ h^{-1}) in peptide L78−F98 slow in the equilibrium mixture of Michaelis complexes relative to the HGPRT·GMP·Mg^{2+} complex (Table 1). Two additional amide protons with very fast exchange rates ($k > 100$ h^{-1}) and one with a fast exchange rate (10 $h^{-1} < k < 100$ h^{-1}) slow in the transition-state analogue complex.

Exchange in Peptide I99−L121. Compared to that in the HGPRT·GMP·Mg^{2+} complex, the extent of deuterium incorporation into peptide I99−L121 decreases in the equilibrium mixture of Michaelis complexes and the transition-state analogue complex (Figure 5B). Two additional protons are protected in the equilibrium mixture of Michaelis complexes after H/D exchange for 60 min, and four protons in the transition-state analogue complex. The exchange rates of amide hydrogens in the transition-state analogue complex of HGPRT differ significantly from those of the equilibrium mixture of Michaelis complexes or of the GMP-bound complex (Figure 6B). Compared to that in the HGPRT·GMP·Mg^{2+} complex, the very fast exchange rate ($k > 100$ h^{-1}) of one amide proton slows in the equilibrium mixture of Michaelis complexes (Table 1). Interestingly, binding ImmGP to HGPRT changes four amide hydrogens with very fast exchange rates ($k > 100$ h^{-1}) and another one with a fast exchange rate (10 $h^{-1} < k < 100$ h^{-1}) into the ranges of either slow exchange rates (0.1 $h^{-1} < k < 10$ h^{-1}) or very slow exchange rates ($k < 0.1$ h^{-1}).

Exchange in Peptide I131−L145. The consequence of binding Michaelis substrates and transition-state analogue on the extent and rate of H/D exchange distinguishes peptide I131−L145 from the two peptides described above. There are no significant differences in the extent of deuterium incorporation between the GMP-bound form and the equilibrium mixture of Michaelis complexes of HGPRT. In the HGPRT·ImmGP·$MgPP_i$ complex, two amide protons are protected from solvent access at the 10 min period of exchange and one amide proton is protected at a 60 min period of exchange, relative to the GMP-bound complex and the equilibrium mixture of Michaelis complexes (Figure 5C). The very fast exchange rate ($k > 100$ h^{-1}) of one amide hydrogen and the fast exchange rate (10 $h^{-1} < k < 100$ h^{-1}) of another in the mixture of Michaelis complexes slow specifically in the transition-state analogue complex (Table 1).

DISCUSSION

Solvent H/D exchange provides an experimental approach to protein dynamics in HGPRT that is not available through other methods. Amide protons in dipeptides are known to exchange at rates of >10 min^{-1} with solvent at neutral pH, but are shielded to a remarkable extent when engaged in

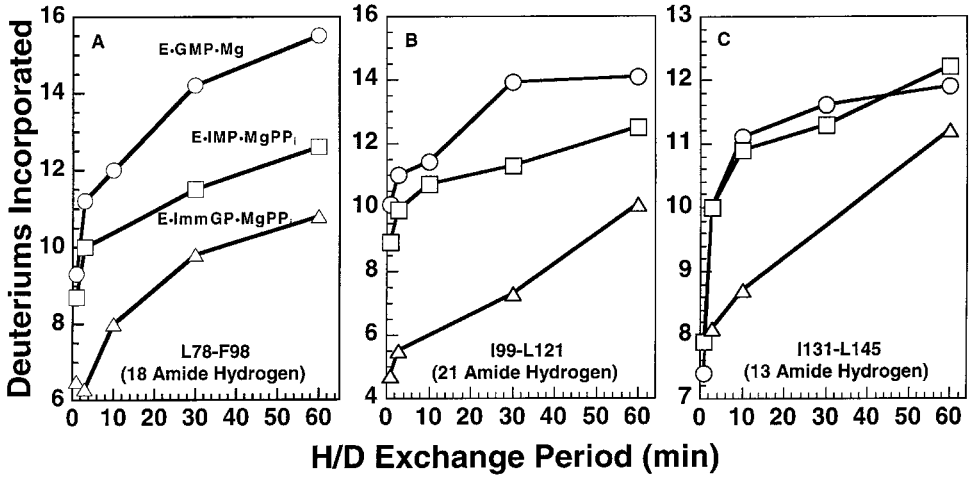

FIGURE 5: Deuterium incorporation at peptide amide positions as a function of time in peptides L78−F98 (A), I99−L121 (B), and I131−L145 (C): GMP and Mg^{2+} (○), IMP and $MgPP_i$ (□), and ImmGP and $MgPP_i$ (△).

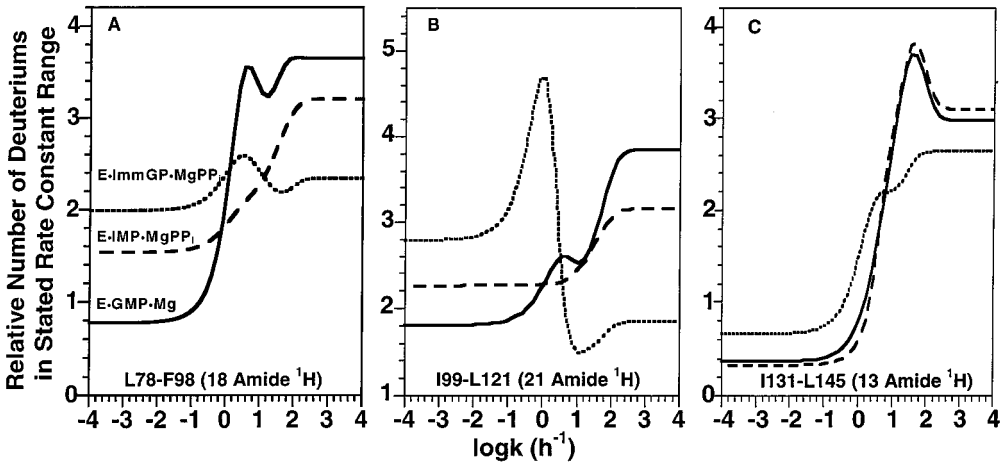

FIGURE 6: H/D exchange rate constant distribution derived from the H/D exchange time courses shown in Figure 5 after subjecting the samples to maximum entropy method analysis (*9*), for peptides L78−F98 (A), I99−L121 (B), and I131−L145 (C): HGPRT·GMP·Mg^{2+} (—), HGPRT·IMP·$MgPP_i$ (− − −), and HGPRT·ImmGP·$MgPP_i$ (···) complexes. The total number of backbone amide hydrogens for each segment is indicated in each panel. The ordinate is scaled so that the total area under each peak corresponds to the number of amide hydrogens with the exchange constants on the abscissa for the peak. Plateau values correspond to rate constants beyond the abscissa scales.

Table 1: Number[a] of Amide Hydrogens with Different Exchange Rates (Figure 6)

Peptide L78−F98 (18 Amide Hydrogens)					
enzyme complex	$k > 100$	$10 < k < 100$	$1 < k < 10$	$0.01 < k < 1$	$k < 0.01$
HGPRT·GMP·Mg^{2+}	8	3	3	1.5	1.5
E·IMP·$MgPP_i$ ⇌ E·Hx·MgPRPP	7	3	2	3	3
HGPRT·ImmGP·$MgPP_i$	5	2	3	4	4
Peptide I99−L121 (21 Amide Hydrogens)					
enzyme complex	$k > 100$	$10 < k < 100$	$0.1 < k < 10$	$k < 0.1$	
HGPRT·GMP·Mg^{2+}	8	3	4.5	5.5	
E·IMP·$MgPP_i$ ⇌ E·Hx·MgPRPP	7	3	4	7	
HGPRT·ImmGP·$MgPP_i$	4	2	6.5	8.5	
Peptide I131−L145 (13 Amide Hydrogens)					
enzyme complex	$k > 100$	$10 < k < 100$	$0.1 < k < 10$	$k < 0.1$	
HGPRT·GMP·Mg^{2+}	6.5	3.5	2	1	
E·IMP·$MgPP_i$ ⇌ E·Hx·MgPRPP	6.5	3.5	2	1	
HGPRT·ImmGP·$MgPP_i$	5.5	2.5	3	2	

[a] The value reported is the number of exchanging amide hydrogen atoms within that exchange rate class (see Figure 6).

hydrogen bonds, when buried in the interior of a protein, or at acidic pH values (*35*). For an amide hydrogen to exchange with solvent deuterium, direct solvent access or a proton transfer bridge is required. Comparison of global exchange indicates the degree of order and solvent access to the peptide backbone, while exchange information for individual peptides reveals loop motion in complexes defined by other structural methods. Any change in protein conformation that maintains amides in bound forms will minimize solvent exchange. Tighter interactions that accompany transition-state analogue complex formation are expected to result in a reduction in residue mobility and the extent of solvent exchange for those peptides involved in the ensemble of transition-state interactions.

HGPRT Complexes. Excess GMP used in H/D exchange placed >99% of the protein into the HGPRT·GMP·Mg^{2+} complex, a form previously characterized by crystallographic studies (*18*, *20*). In the Michaelis complex, IMP and $MgPP_i$ bound to HGPRT react at 200 s^{-1} to give bound hypoxanthine and MgPRPP, and the on-enzyme mixture equilibrates rapidly ($K_{internal} = 17$) relative to product release. The K_m for IMP is 5.4 μM, also ensuring that >99% of the enzyme is in the form of these complexes (*18*). Although no crystal structure is available for this dynamic complex, several substrate analogue structures that approximate the Michaelis complexes are available (*22*, *23*). ImmGP is an inhibitor of HGPRT with a K_i^* of 4.6 nM in the presence of $MgPP_i$, and the structure of the HGPRT·ImmGP·$MgPP_i$ complex has been determined crystallographically (*13*). The transition-state analogue complex is expected to trap the conformational properties that HGPRT exhibits at the transition state, whereas the equilibrium mixture will be populated by the two Michaelis complexes. Ground-state interactions in the Michaelis complexes might be expected to partially order the protein complex, while the ImmGP complex represents the trapping of $\Delta\Delta G^{\ddagger}$ in a stable complex. Therefore, differences in H/D exchange reflect the differing characteristics of the peptides in Michaelis and transition-state conformations. The two pre-Michaelis complexes, unliganded enzyme and the HGPRT·GMP·Mg^{2+} complex, provide comparative information for solvent access.

Global Exchange. Global exchange kinetics clearly indicated that 160 amide hydrogen atoms were replaced with deuterium after exchange for 60 min in HGPRT alone, 154

in the HGPRT·GMP·Mg^{2+} complex, 139 in the equilibrium mixture of Michaelis complexes, and 126 in the HGPRT·ImmGP·$MgPP_i$ complex. Compared to free HGPRT, 21 and 34 amide protons are inhibited from solvent exchange in the equilibrium mixture of Michaelis complexes and in the transition-state analogue complex, respectively. Since the catalytic site is fully occupied in both the Michaelis complexes and the ImmGP complex, the additional 13 sites of exchange represent transition-state features that order and stabilize peptide motions to prevent solvent access. Protein ordering by transition-state analogue binding supports the findings that transition-state analogues greatly facilitate crystallizations of ribosyltransferases and give highly ordered crystals (e.g., refs *4*, *12*, *13*, and *36*). That sequential filling of the catalytic sites provides an increasing level of solvent exclusion from the protein, and a more compact structure is apparent by comparison of the X-ray structures (panels B and C of Figure 1 and panels C and D of Figure 7). Catalytic site loops, surface protein loops, and subunit interface contacts all become closer and more ordered with a bound transition-state inhibitor. These increases in structural stability are reflected in reduced levels of solvent exchange.

Peptide-Specific Exchange. The H/D exchange into specific peptides identifies peptides of HGPRT that respond to the formation of the transition-state analogue complex as compared to Michaelis complexes. Peptides L78−F98, I99−L121, and I131−L145 are indicated in the subunits of the HGPRT·ImmGP·$MgPP_i$ and HGPRT·GMP·Mg^{2+} complexes (Figure 7A,B). These peptides are examples that demonstrate altered H/D exchange properties in response to catalytic site filling. However, the reader is reminded that many peptides demonstrate no H/D exchange differences. Quiescent peptides often are core structural elements, maintained in hydrophobic environments in all complexes. Other peptides gave moderate exchange rates in both complexes, and some short peptides were only represented in the fully exchanged form.

Exchange properties of the amides in each peptide can be correlated with the structural factors involved in solvent exchange, namely, solvent access, hydrogen bonding, mobility, and exchange dynamics for catalytic site ligands. Figure 8 correlates the data from X-ray structures of the HGPRT·ImmGP·$MgPP_i$ and HGPRT·GMP·Mg^{2+} complexes. Each amide group of the three peptides is evaluated for solvent accessible surface area, the length of any identifiable hydrogen bond, and the crystallographic *B*-factor. The solvent exchange dynamics are interpreted by comparison of Figures 5, 7, and 8.

Catalytic Loop. Residues I99−L121 (green in panels A and B of Figure 7) constitute strand $\beta 4'$, strand $\beta 5$, helix $\alpha 4$, and their connecting turn (*13*). This "catalytic" loop is located on the exterior of the enzyme tetramer, where solvent accessibility is high. In the human HGPRT·GMP·Mg^{2+} structure, this loop is flexible, disordered, and oriented away from the active site (Figure 1C; *20*). The X-ray structure of the HGPRT·ImmGP·$MgPP_i$ complex (*13*) and the complex of the K68A mutant of human HGPRT with PRPP, Mg^{2+}, and the nonproductive base analogue HPP (*37*) both show the loop in a closed position over the active sites. In the K68A HGPRT·MgPRPP·HPP complex, $\alpha 4$, formed by residues 116−123, is shifted toward the core of the protein, thus bringing residues 100−115 of the catalytic loop closer to the active site.

In the unproductive Michaelis HGPRT·MgPRPP·HPP complex, the loop is closed without significant structural reordering events and, though more closed, is structurally related to the open loop of the HGPRT·GMP·Mg^{2+} complex (*37*). The conformation of the I99−L121 peptide in the present mixture of Michaelis complexes causes a modest decrease in the extent of H/D exchange compared to that in the HGPRT·GMP·Mg^{2+} complex. These small changes are consistent with the solvent-exposed location of the loop in the HGPRT·MgPRPP·HPP complex, and the lack of conformationally specific hydrogen bonds. In contrast to complexes that mimic the Michaelis complex, the HGPRT·ImmGP·$MgPP_i$ complex reveals catalytic loop movement of ~25 Å to interact closely with the active site. The main chain nitrogens of both Ser103 and Tyr104 are in hydrogen bonds with an oxygen of PP_i (Figure 1B; *13*). This loop now forms a two-stranded antiparallel β-structure ($\beta 4'$ and $\beta 5$) with nine new hydrogen bonds formed between the amide nitrogens and other atoms of the loop (Figure 7A, middle panel). These nine hydrogen bonds do not exist in the HGPRT·GMP·Mg^{2+} or the K68A HGPRT·MgPRPP·HPP complexes. They uniquely characterize the transition-state analogue complex. The amide nitrogen atoms of residues I99−L121 have less solvent accessible surface in the HGPRT·ImmGP·$MgPP_i$ complex than in the HGPRT·GMP·Mg^{2+} complex (Figure 8A, top panel). Amide nitrogens of residues 100−104 and 107−112 each demonstrated >2 $Å^2$ solvent access in the GMP complex, but almost none in the transition-state complex.

After binding the transition-state analogue complex, the reduction in exchange kinetics in the I99−L121 segment is profound. Following 60 min in D_2O, only 10 of the 21 protons are exchanged and the rate of exchange is also slowed. We find that solvent exchange into this loop involves the dynamic conversion between open exchangeable enzyme forms and the closed form in contact with the transition-state analogue. The mechanism of exchange inhibition is transition-state-analogue-induced stalling of protein loop dynamics. Ten of the peptide nitrogens of I99−L121 have no hydrogen bond partner in the transition-state analogue complex (Figure 8A, top and middle panels). These amides are expected to exchange provided that solvent access occurs. Considering both amide hydrogen bonds and solvent access, it is predicted that I99−L121 in complexes of HGPRT·GMP·Mg^{2+} and HGPRT·ImmGP·$MgPP_i$ should rapidly exchange 8 or 6 protons respectively (Table 4). We find that 10 and 4 H/D exchanges occur by 1 min, and that 14 and 7 H/D exchanges have occurred into the respective complexes at 30 min (Figure 5B). Thus, dynamic fluctuations of the loop in HGPRT·GMP·Mg^{2+} allow substantial additional exchange over that predicted from rigid body considerations. In contrast, exchange is restricted to the expected number of amides in the transition-state analogue complex. During the 30−60 min period, three more H/D exchanges occur in the transition-state analogue complex, with no additional exchange in the GMP complex. Thus, dynamic H/D exchange to the loop in the transition-state complex is slow.

Ligand exchange rates for GMP and ImmGP and structural B-factors help explain the solvent exchange dynamics. Rate constants for the tight-binding slow-onset HGPRT·ImmGP·$MgPP_i$ complex are 0.6 min^{-1} for formation and 0.052 min^{-1}

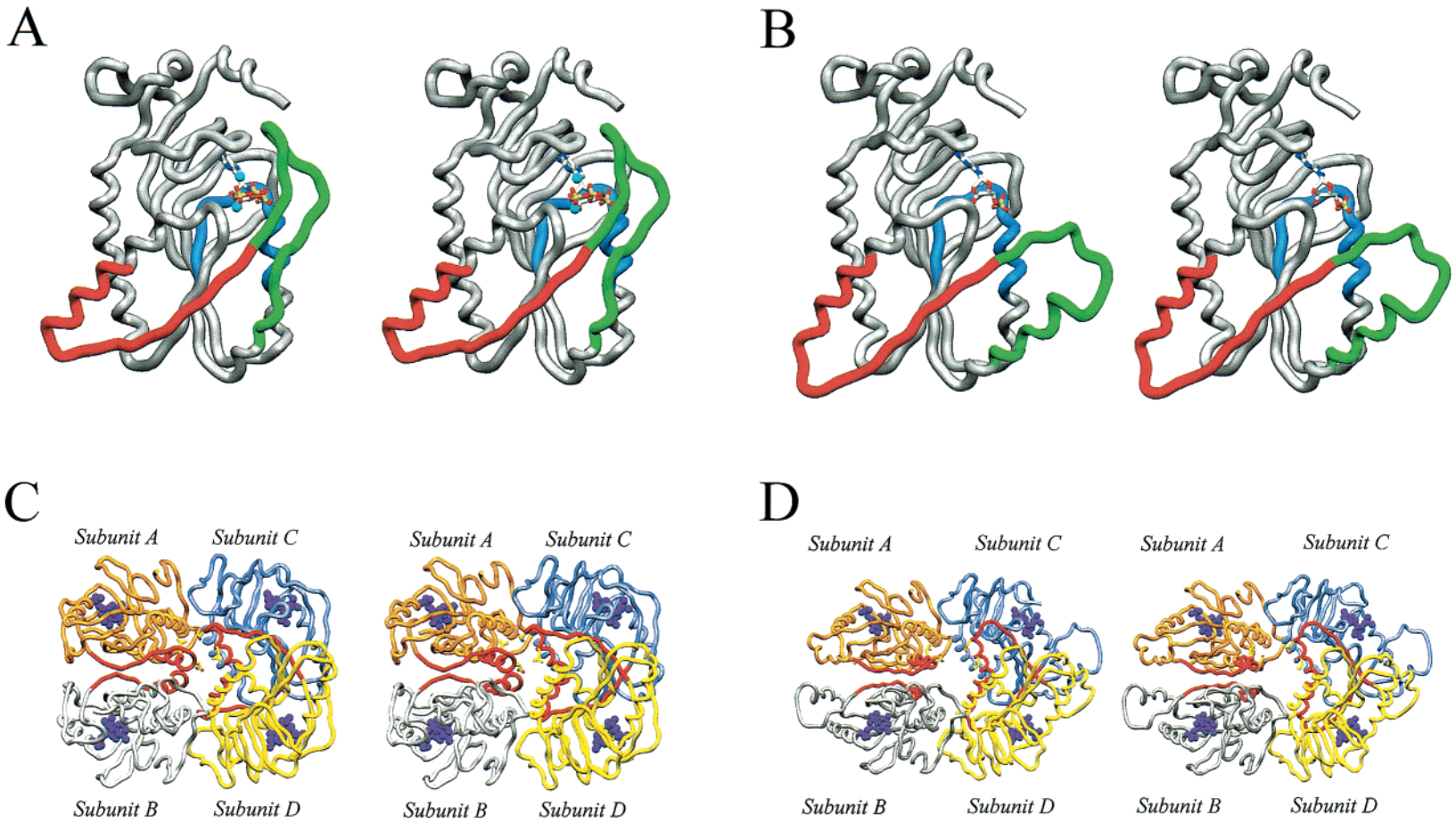

FIGURE 7: (A) Stereoview of the three-dimensional structure of the human HGPRT subunit containing bound ImmGP and $MgPP_i$. Peptide segments are colored as follows: red, residues 78−98; green, residues 99−121; and blue, residues 131−145. Phosphorus is yellow, oxygen red, nitrogen blue, and Mg^{2+} blue spheres. (B) Stereoview of the three-dimensional structure of the human HGPRT subunit containing bound GMP and Mg^{2+}. Only the GMP molecule is shown in the catalytic site. The color scheme is the same as in panel A. (C) Arrangement of the subunits in the tetramer of the HGPRT·ImmGP·$MgPP_i$ complex. A space filling representation of ImmGP is shown in purple. Subunits A−D are gold, gray, light purple, and yellow, respectively, and peptide segments of residues 78−98 in subunits A−D are red. (D) Arrangement of subunits in the tetramer of the HGPRT·GMP·Mg^{2+} complex. GMP is purple, and subunits are colored as in panel C.

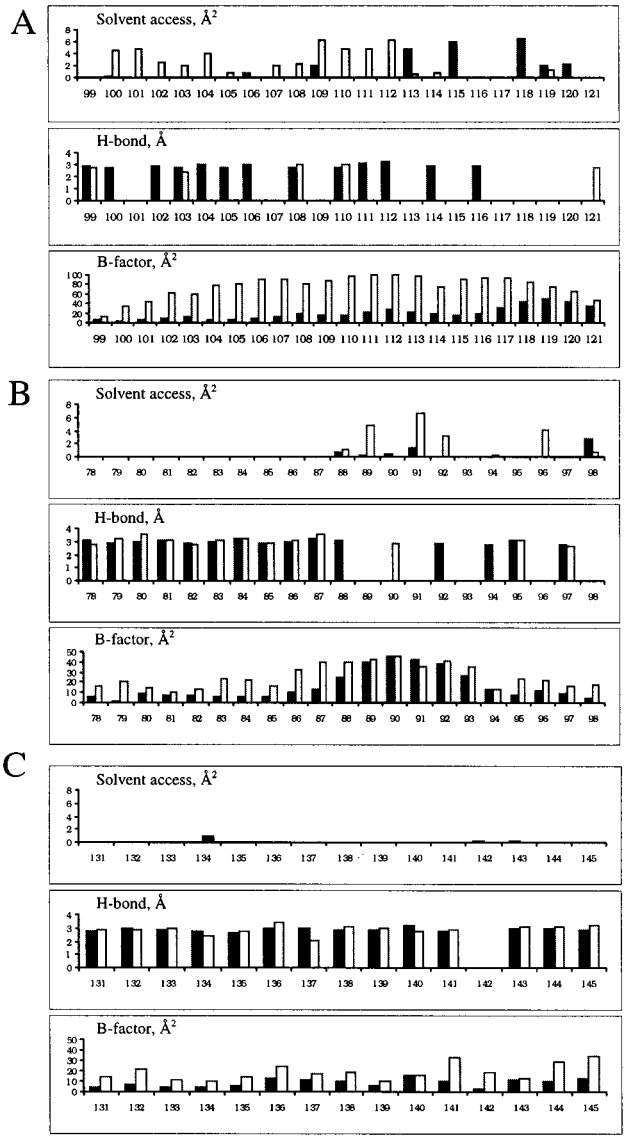

FIGURE 8: Solvent accessibility, hydrogen bond lengths, and crystallographic *B*-factors for specific amide nitrogens (H/D exchange sites) in peptides from HGPRT. These parameters are shown both for peptides from the HGPRT·GMP·Mg^{2+} complex (white bars) and for peptides from the HGPRT·ImmGP·$MgPP_i$ complex (black bars): (A) residues 99−121, (B) residues 78−98, and (C) residues 131−145. For each amide peptide nitrogen, the solvent accessibility (top histogram in panels A−C), hydrogen bond length (middle histogram in panels A−C), and crystallographic *B*-factor (bottom histogram in panels A−C) were calculated from the relevant PDB files (*13*, *20*). For the HGPRT·GMP·Mg^{2+} complex, some hydrogen bonds (mostly in peptide I99−L121) exhibit unusual geometry. Note that peptide I131−L145 has no solvent access, but still participates in H/D exchange (Figure 5C).

for its relaxation (*19*). The relaxation step therefore has a $t^1/_2$ of 13.3 min, requiring more than 60 min to fully equilibrate with solvent. High B-factors for HGPRT·GMP·Mg^{2+} and lower values of HGPRT·ImmGP·$MgPP_i$ correlate with the observed exchange profile (Figure 8A, lower panel). Individual amide protons cannot be assigned by this exchange method. However, the overall data show exchange rate protection factors of at least 100, and probably much higher, for the four amide protons remaining unexchanged at 60 min in the transition-state analogue complex but not the GMP complex. These factors suggest a minimal interaction strength of 2.8 kcal/mol. In the normal transition state, this energy would be available for offsetting the demands of chemistry.

Table 2: Interactions between Subunit A and Subunit D via van der Waals Contacts in the Human HGPRT·ImmGP·$MgPP_i$ Complex[a]

atom 1	residue in subunit A	atom 2	residue in subunit D	distance (Å)
CD2	Leu84	CB	Asn87	3.7
CD2	Leu84	OD1	Asn87	3.8
CD2	Leu84	CG	Asn87	3.9
CB	Asn87	CD2	Leu84	3.7
OD1	Asn87	CD2	Leu84	3.9
CG	Asn87	CD2	Leu84	3.9

[a] The positions of the side chains of Leu84 and Asn87 at those interfaces can be seen by careful inspection of the subunit contact regions in panels C and D of Figure 7.

Table 3: Hydrogen Bond Distances in Human HGPRT·GMP·Mg^{2+} and HGPRT·ImmGP·$MgPP_i$ Complexes

atom 1	atom 2	residue	distance with GMP (Å)[a]	distance with ImmGP (Å)[b]
O2P	N	Thr141	2.9	2.7
	OG1	Thr141	2.9	2.8
O3P	N	Thr138	2.9	2.9
	OG1	Thr138	2.6	2.6
O1P	N	Gly139	3.1	2.8
	N	Asp137	3.1	3.1
O3′	OE1	Glu133	2.9	2.7
O2′	OE1	Asp134	4.4	2.5

[a] From ref *20*. [b] From ref *13*.

Subunit Interface. Peptide L78−F98 (red in Figure 7A,B) is contiguous with the catalytic site loop, and its H/D exchange is sensitive to catalytic site filling. When the catalytic site peptide closes in response to ImmGP, the change is coupled to a secondary conformational motion in peptide L78−F98, changing its disposition at the subunit interface (Figure 7C,D). The α3−β4 turn (residues 86−91) is involved in the interactions at the dimer interface between subunits A and B (or C and D) (Figure 7C,D). Comparing the X-ray structures of the HGPRT·GMP·Mg^{2+} complex with the HGPRT·ImmGP·$MgPP_i$ complex, we find no significant differences in the interaction at the dimer interface between subunits A and B (or C and D). Surprisingly, however, we found that the α3−β4 turn is also involved in the interaction of the third dimer interface between nonadjacent subunits A and D (or B and C) in the HGPRT·ImmGP·$MgPP_i$ complex (Table 2 and Figure 7C,D). The side chains of residues Leu84 and Asn87 in subunit A make 3.7 and 3.9 Å van der Waals contacts with the side chains of residues Asn87 and Leu84 in subunit D, respectively. The shortest distance between Cα atoms of helices α3 in subunits A and D (residues 87A and 84D) is 7.4 Å. The tetramer of the HGPRT·GMP·Mg^{2+} complex (generated by application of the crystallographic 2-fold axis to the dimeric asymmetric unit) shows no interaction between the interfaces of subunits A and D (or B and C). The shortest distance between helix α3 in subunit A and helix α3 in subunit D is 12.6 Å, an increase of 5.2 Å as compared to that in the HGPRT·ImmGP·$MgPP_i$ complex.

The X-ray structure of the tetrameric K68A mutant HGPRT·MgPRPP·HPP complex (*37*) (generated by applying the crystallographic 2-fold axis to the dimer) shows a single van der Waals contact between subunit A and subunit D. Residue Asn87 in subunit A makes van der Waals contact with its counterpart in subunit D with a distance of 3.5 Å.

Table 4: Exchangeable Amide Protons Predicted by Rigid Body Analysis and Observed by H/D Exchange

	exchange predicted from solvent access[a]		exchange predicted from H bonds[b]		exchange predicted from H bonds and solvent access[c]		30 min observed exchange	
peptide	GMP	ImmGP	GMP	ImmGP	GMP	ImmGP	GMP	ImmGP
I99−L121	11	6	18	10	8	6	14	7
L78−F98	4	2	8	6	4	2	14	10
I131−L145	0	0	1	1	0	0	12	9

[a] Solvent accessible amide nitrogens are defined as those having solvent access greater than 1.5 Å^2 as determined with a standard probe with a radius of 1.4 Å. [b] Exchangeable amide protons are those without an appropriate hydrogen bond acceptor within 3.2 Å of the nitrogen for the HGPRT·ImmGP·$MgPP_i$ structure or (because of large *B*-factors in that complex) within 3.5 Å in the HGPRT·GMP·Mg^{2+} structure. [c] Predicted H/D exchange sites from rigid body analysis assuming solvent access of greater than 1.5 Å^2 and no hydrogen bond acceptor within the distances defined in footnote b.

The shortest distance between helix α3 in subunit A and helix α3 in subunit D is 8.6 Å, an increase of 1.2 Å as compared to that in the complex with ImmGP. Therefore, binding ImmGP to HGPRT tightens the subunit contacts and reduces the diameter of the tetramer.

An analysis of solvent access, hydrogen bonding, and *B*-factors in individual amide nitrogens of peptide L78−F98 is shown in Figure 8B. Hydrogen bond patterns and solvent access predict only four and two H/D rapid exchanges from rigid body analysis of this peptide in the HGPRT·GMP·Mg^{2+} and HGPRT·ImmGP·$MgPP_i$ complexes, respectively (Table 4). We find nine and six exchanges have occurred by 1 min (Figure 5A), and 16 and 10 H/D exchanges are observed after 60 min. In this peptide, dynamics dominate static structural influences on exchange, and the subunit interface remains in dynamic fluctuation, permitting solvent access beyond predictions based on X-ray crystallography. Although this peptide receives weaker immobilization and protection from transition-state formation than does the contiguous catalytic loop, it provides an impressive example of the extent of remote conformational interactions coupled to transition-state analogue binding. The role of this specific change in conformation in the achievement of the transition state for catalysis is not known, but it clearly strengthens the subunit interactions.

Phosphate Binding Loop. Residues I131−L145 constitute strand β6, helix α5, and the sharp turn connecting β6 and α5 (*12*, *20*) (blue in Figure 7A,B). The sharp turn is formed by residues Asp137−Thr141. Main chain nitrogens of Thr138, Gly139, and Thr141 are oriented toward the 5′-phosphate group of the substrate within hydrogen-bonding distance (Figure 1B). These hydrogen bond distances are not significantly different (within 0.3 Å) in human HGPRT·GMP·Mg^{2+} and HGPRT·ImmGP·$MgPP_i$ complexes (Figure 1B,C and Table 3). Unlike peptides L78−F98 and I99−L121, peptide I131−L145 is positioned on the inside of the catalytic pocket with solvent access denied by the presence of either GMP or ImmGP. Analysis of the complexes (Figure 8C) indicates that none of these amides are expected to undergo H/D exchange on the basis of hydrogen bond patterns and solvent access as long as the catalytic site cavity is occupied by a nucleotide 5′-phosphate. Experimentally, we see seven to eight deuteriums exchanged in the first minute, and 12 and nine deuteriums exchanged into the peptide in 30 min in the GMP and ImmGP complexes, respectively. GMP exchanges from the catalytic site at a rate of 13 s^{-1} (*18*), thus providing dynamic solvent access and H/D exchange. However, the robust exchange of nine deuteriums into peptide I131−L145 of the ImmGP complex in 30 min cannot be explained on the basis of the ImmGP exchange rate of 0.052 min^{-1} (*19*). Rather, the result suggests that the two water molecules hydrogen-bonded to 5′-phosphate oxygens (oxygens that share hydrogen bonds from amides of Asp137, Thr138, Gly139, and Thr141) provide a proton exchange bridge to permit H/D exchange that is more rapid than ligand release (Figure 1B). We suggest that the amides within proton exchange distance of these two catalytic site waters are likely candidates for rapid exchange.

Summary. H/D exchange in the human HGPRT·ImmGP·$MgPP_i$ complex provides both conformational and dynamic properties of the tightly closed catalytic conformation. Binding ImmGP to HGPRT protects more amide protons from solvent exchange than binding GMP or the Michaelis complexes. Peptic peptide analysis allows the mapping of solvent access to specific peptides of the HGPRT subunits. The extent and rate of H/D exchange depend on the amide bond environment, access provided by loop movement, ligand exchange, and proton exchange paths. Exchange into the loop covering the catalytic site (peptide I99−L121) is surprisingly resistant in the HGPRT·ImmGP·$MgPP_i$ complex. Exchange in this loop is initially governed by rigid body properties in the HGPRT·ImmGP·$MgPP_i$ complex, with a subsequent slow exchange due to loop opening related to ImmGP exchange. In the GMP complex, dynamic loop opening is fast and adds solvent access sites to rigid body exchange properties. The loop that transmits conformational information to the tetramer interface (peptide L78−F98) has limited solvent access, but a time-dependent H/D exchange occurs at almost all amides in the weakly bound HGPRT·GMP·Mg^{2+} complex. Almost half of these amides are protected from exchange by the ImmGP·$MgPP_i$ species, revealing structural dynamics changes transmitted to the tetramer interface. A buried catalytic site loop (residues I131−L145) has virtually no solvent access when 5′-phosphonucleotides are bound. H/D exchange occurs much faster than ligand exchange or loop relaxation in the HGPRT·ImmGP·$MgPP_i$ complex, and provides evidence that trapped catalytic site waters form proton transfer bridges to nearby amides. This analysis provides new details for the mechanism of H/D exchange into enzymatic complexes trapped with transition-state analogues.

ACKNOWLEDGMENT

F.W. thanks Yiming Xu for helpful discussion and Zhongqi Zhang for providing programs for reading the centroid values of peaks and for subjecting the deuterium uptake versus time profiles to MEM analysis. We thank Beth Vonbaur for skillful preparation of human HGPRT.

REFERENCES

1. Pauling, L. (1948) *Am. Sci. 36*, 50−58.
2. Albery, W. J., and Knowles, J. R. (1976) *Biochemistry 15*, 5631−5640.
3. Snider, M. J., Gaunitz, S., Ridgway, C., Short, S. A., and Wolfenden, R. (2000) *Biochemistry 39*, 9746−9753.
4. Shi, W., Munagala, N. R., Wang, C. C., Li, C. M., Tyler, P. C., Furneaux, R. H., Grubmeyer, C., Schramm, V. L., and Almo, S. C. (2000) *Biochemistry 39*, 6781−6790.
5. Zhang, Z., and Smith, D. L. (1993) *Protein Sci. 2*, 522−531.
6. Katta, V., and Chait, B. T. (1993) *J. Am. Chem. Soc. 115*, 6317−6321.
7. Engen, J., and Smith, D. (2000) *Methods Mol. Biol. 146*, 95−112.
8. Smith, D., Deng, Y., and Zhang, Z. (1997) *J. Mass Spectrom. 32*, 135−146.
9. Zhang, Z., Li, W., Logan, T. M., Li, M., and Marshall, A. G. (1997) *Protein Sci. 6*, 2203−2217.
10. Schramm, V. L. (1998) *Annu. Rev. Biochem. 67*, 693−720.
11. Miles, R. W., Tyler, P. C., Furneaux, R. H., Bagdassarian, C. K., and Schramm, V. L. (1998) *Biochemistry 37*, 8615−8621.
12. Shi, W., Li, C. M., Tyler, P. C., Furneaux, R. H., Cahill, S. M., Girvin, M. E., Grubmeyer, C., Schramm, V. L., and Almo, S. C. (1999) *Biochemistry 38*, 9872−9880.
13. Shi, W., Li, C. M., Tyler, P. C., Furneaux, R. H., Grubmeyer, C., Schramm, V. L., and Almo, S. C. (1999) *Nat. Struct. Biol. 6*, 588−593.
14. Wang, F., Miles, R. W., Kicska, G., Nieves, E., Schramm, V. L., and Angeletti, R. H. (2000) *Protein Sci. 9*, 1660−1668.
15. Berens, R. L., Krug, E. C., and Marr, J. J. (1995) in *Biochemistry and Molecular Biology of Parasites* (Marr, J., and Muller, M., Eds.) pp 89−117, Academic Press, London.
16. Krenitsky, T. A., Papaioannou, R., and Elion, G. B. (1969) *J. Biol. Chem. 244*, 1263−1270.
17. Ullman, B., and Carter, D. (1995) *Infect. Agents Dis. 4*, 29−40.
18. Xu, Y., Eads, J., Sacchettini, J. C., and Grubmeyer, C. (1997) *Biochemistry 36*, 3700−3712.
19. Li, C. M., Tyler, P. C., Furneaux, R. H., Kicska, G., Xu, Y., Grubmeyer, C., Girvin, M. E., and Schramm, V. L. (1999) *Nat. Struct. Biol. 6*, 582−587.
20. Eads, J. C., Scapin, G., Xu, Y., Grubmeyer, C., and Sacchettini, J. C. (1994) *Cell 78*, 325−334.
21. Jardim, A., and Ullman, B. (1997) *J. Biol. Chem. 272*, 8967−8973.
22. Heroux, A., White, E. L., Ross, L. J., and Borhani, D. W. (1999) *Biochemistry 38*, 14485−14494.
23. Heroux, A., White, E. L., Ross, L. J., and Borhani, D. W. (1999) *Biochemistry 38*, 14495−14506.
24. Brennand, J., Konecki, D. S., and Caskey, C. T. (1983) *J. Biol. Chem. 258*, 9593−9596.
25. Penefsky, H. S. (1979) *Methods Enzymol. 56*, 527−530.
26. Furneaux, R. H., Limberg, G., Tyler, P. C., and Schramm, V. L. (1997) *Tetrahedron 53*, 2915−2930.
27. Furneaux, R. H., Schramm, V. L., and Tyler, P. C. (1999) *Bioorg. Med. Chem. 7*, 2599−2606.
28. Johnson, R. S., and Walsh, K. A. (1994) *Protein Sci. 3*, 2411−2418.
29. Johnson, R. S. (1996) *J. Am. Soc. Mass Spectrom. 7*, 515−521.
30. Wang, F., Scapin, G., Blanchard, J. S., and Angeletti, R. H. (1998) *Protein Sci. 7*, 293−299.
31. Wang, F., Li, W., Emmett, M. R., Hendrickson, C. L., Marshall, A. G., Zhang, Y. L., Wu, L., and Zhang, Z. Y. (1998) *Biochemistry 37*, 15289−15299.
32. Yates, J. R. d., Speicher, S., Griffin, P. R., and Hunkapiller, T. (1993) *Anal. Biochem. 214*, 397−408.
33. Wilson, J. M., Tarr, G. E., Mahoney, W. C., and Kelley, W. N. (1982) *J. Biol. Chem. 257*, 10978−10985.
34. Johnson, G. G., Eisenberg, L. R., and Migeon, B. R. (1979) *Science 203*, 174−176.
35. Molday, R. S., Englander, S. W., and Kallen, R. G. (1972) *Biochemistry 11*, 150−158.
36. Fedorov, A., Shi, W., Kicska, G., Fedorov, E., Tyler, P. C., Furneaux, R. H., Hanson, J. C., Gainsford, G. J., Larese, J. Z., Schramm, V. L., and Almo, S. C. (2001) *Biochemistry 40*, 853−860.
37. Balendiran, G. K., Molina, J. A., Xu, Y., Torres-Martinez, J., Stevens, R., Focia, P. J., Eakin, A. E., Sacchettini, J. C., and Craig, S. P., III (1999) *Protein Sci. 8*, 1023−1031.
38. Tao, W., Grubmeyer, C., and Blanchard, J. S. (1996) *Biochemistry 35*, 14−21.

BI010203F